

Investigation of Thermoelectric Properties of a Two-Dimensional Janus Si₂SbBi and Non-Janus SiSb Using Computational Method Density-Functional Theory

Yusuf Affandi ^{a,*}, Muhammad Yusrul Hanna ^b

^a*Instrumentation and Automation Engineering Faculty of Industrial Technology
Institut Teknologi Sumatera
Lampung Selatan 35365, Indonesia*
^b*Research Center for Quantum Physics
National Research and Innovation Agency (BRIN)
South Tangerang 15314, Indonesia*

Abstract

Two-dimensional materials are of considerable interest owing to their unique electronic and thermal properties. In this study, we investigate the thermoelectric potential of two-dimensional Janus Si₂SbBi and compare it with a non-Janus SiSb based on the first-principles density functional theory (DFT) band structure calculations. According to the first-principles calculations, both materials exhibit semiconductor properties with bandgaps of 0.728 eV (Janus Si₂SbBi) and 0.82 eV (SiSb), respectively. Having information on the energy band structure, we evaluated thermoelectric properties using the Boltzmann transport equations as a function of Fermi energy as implemented in the BoltzTrap2 code. We find a Seebeck coefficient of 1349 (1342) $\mu\text{V}/\text{K}$ for *p*-type (*n*-type) doping at $T = 300$ K of the Si₂SbBi monolayer. The results of our study present that the Janus Si₂SbBi monolayer possesses a high Seebeck coefficient and electrical conductivity, leading to a substantial power factor (PF) of 4×10^{11} W/K²ms at 300 K. The PF increases with an increase in temperature and has the highest peak value up to 7×10^{11} W/K²ms at 600 K. The results show that the Seebeck coefficient, electrical conductivity, and power factor of the Janus Si₂SbBi monolayer are greater compared to those of the non-Janus SiSb monolayer. Our study presents Janus Si₂SbBi as a potential thermoelectric candidate, highlighting its prospective use in advanced thermoelectric applications.

Keywords: Janus Si₂SbBi, non-Janus SiSb, Boltzmann transport, Seebeck coefficient, power factor.

I. INTRODUCTION

The focus on technological advancement lies in optimizing the efficiency of electronic devices. Minimizing heat energy produced by these devices is essential. Thermoelectric (TE) technology offers a viable solution to address this efficiency concern. This technology reduces the heat energy emitted by electronic devices and transforms it into electrical energy [1]. TE devices function by utilizing the Seebeck effect, where a temperature difference across a TE material generates a voltage difference across it. This voltage difference leads to the conversion of heat into usable electricity [2].

However, finding TE materials is challenging; they need high electrical conductivity with low thermal conductivity. The efficiency of TE materials relies on their dimensionless figure-of-merit (ZT), which can be expressed as (1) [3].

$$ZT = \frac{S^2 \sigma T}{\kappa} \quad (1)$$

Here, the Seebeck coefficient, S , measures the ability to convert temperature differences into voltage, while σ

represents the electrical conductivity, T is absolute temperature, and κ is total thermal conductivity. For years, researchers have prioritized identifying TE materials with higher ZT values. This pursuit has been ongoing for an extended period, emphasizing the search for materials that possess superior TE properties [4]–[6].

Two-dimensional materials like graphene and transition metal dichalcogenides (TMDC) have intrigued researchers with their distinctive properties, as well as their potential for applications in optoelectronics, spintronics, and even TE properties [7]–[9]. In addition to TMDC, several other two-dimensional materials have been reported to have a high ZT , such as the IV-VI Chalcogenides family and Si X ($X = \text{S, Se, N, P, As, Sb, Bi}$) monolayer [10]–[12]. Monolayers like Si X (where $X = \text{S, Se, N, P, As, Sb, Bi}$) exhibit an A₂B₂ chemical structure, which belongs to the IV-V group elements. It has a hexagonal structural form and has been investigated theoretically [10], [12], [13].

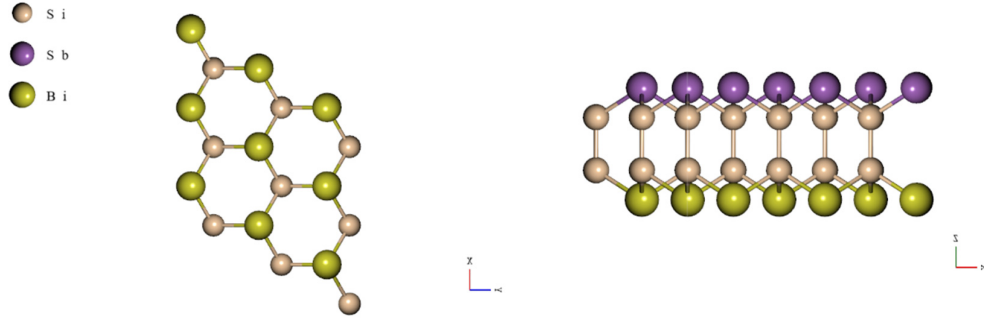
The polar Si₂XY ($X, Y = \text{P, As, Sb, and Bi}$) monolayer system, also known as the Janus Si₂XY monolayer, presents an intriguing area of study. Janus Si₂XY monolayer has a non-centrosymmetric crystal structure due to the difference of group V atoms binding to Si atoms [14], [15]. We hypothesize that its unique crystal structure, in contrast to non-Janus (non-polar) materials, will influence the energy gap and, consequently, its TE properties. Based on this uniqueness, we further

* Corresponding Author.

Email: yusuf.affandi@ia.itera.ac.id

Received: August 24, 2023 ; Revised: December 08, 2023

Accepted: December 15, 2023 ; Published: December 31, 2023


 Figure 1. Atomic structure of Janus Si₂SbBi on (a) top and (b) side view.

investigated the potential of Janus Si₂XY material for TE device applications.

In this work, by using density-functional theory (DFT) calculation implemented in the Quantum ESPRESSO [16], we identified the structure and electronic properties of Janus Si₂SbBi monolayer material. We also use the BoltzTraP2 code [17] to cover the TE properties of this material. Our study also compares the electronic and TE properties of the Janus Si₂SbBi monolayer with the non-Janus system SiSb monolayer. Our results show that the Janus Si₂SbBi monolayer has a greater Seebeck coefficient, electrical conductivity, and power factor compared to the non-Janus SiSb monolayer. This study is the first to report on the promising electrical and TE properties of the Janus Si₂SbBi monolayer, underscoring its potential as a TE material.

II. COMPUTATIONAL METHOD

The Janus Si₂SbBi monolayer has a hexagonal honeycomb structure, which is clearly visible from the top view, where each group V atom is bonded to three Si atoms to build a hexagonal lattice (see Figure 1). The broken centrosymmetry of the crystal structure is due to the difference in the group V atoms (Sb and Bi atoms) bound to Si atoms.

To obtain structure optimization and electronic properties, we perform the DFT calculation implemented in the Quantum ESPRESSO package [16]. The Perdew-Burke-Ernzerhof (PBE) functional of generalized gradient approximation (GGA) [18] is employed as the exchange-correlation function without spin-orbit coupling, while the pseudopotentials are chosen to be ultrasoft [19]. We do not consider spin-orbit coupling in our calculation because it does not investigate phenomena that are significantly influenced by them, such as the Rashba effect, spin Hall effect, spin ballistic, and others. In our DFT calculation, the structure of the Janus Si₂SbBi monolayer is modeled as a periodic slab with a large vacuum layer of 20 Å to eliminate interaction between adjacent layers. In this case, we set a kinetic energy cutoff of 60 Ry, a 12 × 12 × 1 Monkhorst-Pack *k*-mesh to sample Brillouin zone integration, and the crystal geometries were subjected to complete relaxation until the force acting on each atom was below 1 × 10⁻⁵ eV/Å. The optimized structural-related parameters obtained from the calculations are presented in Table 1.

The optimized tetrahedron method was implemented [20] to calculate the DOS, which is defined as the number of states at a given energy.

We obtained the optimized lattice constants for Janus Si₂SbBi monolayer and SiSb monolayer are 4.054 Å and 4.049 Å, respectively. The bond lengths of Si-Sb (d_{Si-Sb}) and Si-Bi (d_{Si-Bi}) for Janus Si₂SbBi monolayer are 2.6454 Å and 2.6453 Å, respectively. For the optimized SiSb monolayer atomic position, we found the bond length of Si-Sb atoms is 2.5952 Å. In general, we find that these parameters are in good agreement with previous studies [14].

Having information about the band structure, the TE properties of this material were calculated using the Boltzmann transport equation along with the constant relaxation time approximation (CRTA) [21] implemented in the BoltzTraP2 code [17]. Here, the relaxation time (τ) of electrons was fixed to 10 fs as proposed by [22]. The calculation of transport parameters is carried out using temperature variations ranging from 300 K to 600 K.

Based on the Boltzmann transport equation, the Seebeck coefficient and electrical conductivity can be expressed as (2) and (3),

$$S(\mu, T) = \frac{ek_B}{\sigma} \int d\varepsilon \left(-\frac{\partial f_{\mu}(\varepsilon, T)}{\partial \varepsilon} \right) \Xi(\varepsilon) \frac{\varepsilon - \mu}{k_B T} \quad (2)$$

$$\sigma(\mu, T) = e^2 \int d\varepsilon \left(-\frac{\partial f_{\mu}(\varepsilon, T)}{\partial \varepsilon} \right) \Xi(\varepsilon) \quad (3)$$

where k_B is Boltzmann Constant and μ is the chemical potential. The transport distribution function $\Xi(\varepsilon)$ and

TABLE 1
STRUCTURAL-RELATED PARAMETERS IN JANUS Si₂SbBi AND NON-JANUS SiSb MONOLAYER. THE LATTICE PARAMETER IS DENOTED AS a (Å), WHILE d_{Si-Sb} AND d_{Si-Bi} REPRESENTS BOND LENGTHS BETWEEN THE SI ATOM AND THE Sb AND Bi ATOMS, RESPECTIVELY

Material	a (Å)	d_{Si-Sb} (Å)	d_{Si-Bi} (Å)	Ref.
Si ₂ SbBi monolayer	4.054	2.645	2.6453	This work
	4.049	-	-	[14]
	4.010	2.630	2.680	[15]
SiSb Monolayer	4.086	2.595	-	This work
	4.010	-	-	[23]

the Fermi Dirac distribution function $f(\varepsilon, \mu, T)$ are given by (4) and (5) [24], [25].

$$f(\varepsilon, T) = \frac{1}{\exp\left(\frac{\varepsilon - \mu}{k_B T}\right) + 1} \quad (4)$$

$$\mathcal{E}(\varepsilon) = \sum_k \tau_k \delta(\varepsilon - \varepsilon_k) v_k^\alpha v_k^\beta \quad (5)$$

III. RESULTS AND DISCUSSION

The electronic band structure of the Janus Si₂SbBi monolayer is shown in Figure 2(b). The Janus Si₂SbBi monolayer exhibits the characteristics of an indirect gap semiconductor with an energy gap of 0.82 eV. We observed that there are two local minima in the conduction band located in the M and K valleys and the unoccupied state on the VBM at the Γ point. Indirect-gap semiconductor properties are also observed in the non-Janus systems, such as the SiSb monolayer (Figure 2(a)) with an energy gap of 0.728 eV. This result is consistent with recent observations of the electronic structure of 2D V-group atoms based on Si atoms monolayer (Table 2).

To estimate the TE properties of the Janus Si₂SbBi monolayer, We employ the BoltzTraP2 code [17], which is represented by the Boltzmann transport equation and the constant relaxation time approximation (CRTA) [21]. We acquired the transport parameters of the Janus Si₂SbBi monolayer, including thermal conductivity (κ_e) and electrical conductivity (σ_e). These parameters were measured as a function of chemical potential (μ) at varying temperatures (T), as shown in Figure 3. We have chosen the ideal temperature ranges of 300 K to 600 K to avoid any phase changes. The chemical potential indicates the doping level or carrier concentration in the system [26]. In this system, a positive value of $\mu - E_f$ indicates n -type doping, whereas a negative value suggests p -type doping.

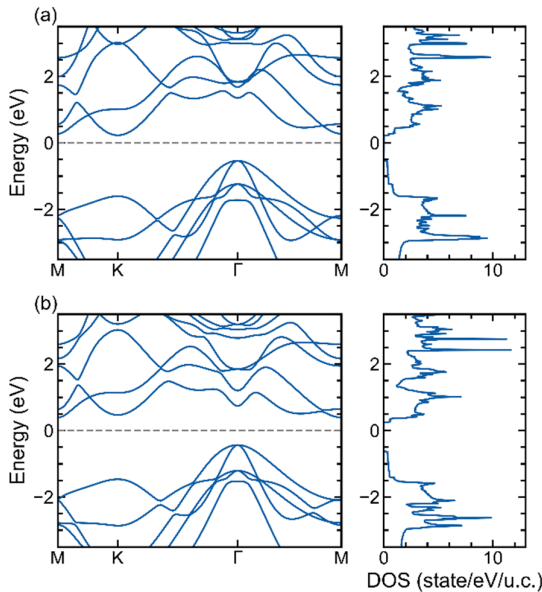


Figure 2. The electronic band structure and DOS of SiSb (a) and Janus Si₂SbBi (b) monolayer, respectively.

TABLE 2
ELECTRONIC AND THERMOELECTRIC PARAMETERS AT ROOM TEMPERATURE RESULT FROM THIS WORK AND OTHER STUDIES FOR COMPARISON

Material	E_g (eV)	p -type (n -type) ($\mu V/K$)	Ref
Janus Si ₂ SbBi Monolayer	0.82	1349(1342)	This work
SiSb Monolayer	0.728	1198(1198)	This work
SiBi Monolayer	0.67	1028(1088)	[13]
Be ₃ C ₂	-	151	[28]
Be ₃ Si ₂	-	136	[28]
Be ₃ Sn ₂	-	101	[28]
Be ₃ Ge ₂	-	140	[28]
ScP monolayer	0.18	1182(1223) under strain 14%	[24]
ScAs monolayer	0.28	950(929) under strain 14%	[24]

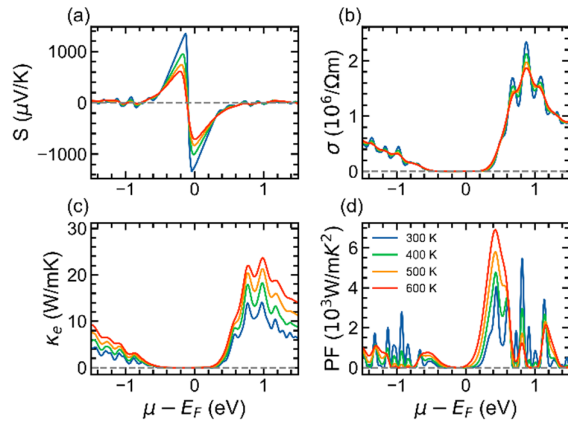


Figure 3. Seebeck coefficient (a), Electrical conductivity (b), Thermal conductivity (c), and Power Factor (d) of Janus Si₂SbBi monolayer.

Figure 3(b) shows an increase in electrical conductivity of the Janus Si₂SbBi monolayer with increasing carrier concentration and a decrease with rising temperature. This was due to a reduction in the relaxation time [25]. The highest peak of electrical conductivity is $\sigma = 1.75 \times 10^6 / \Omega m$ at ambient temperature. Comparable findings were also achieved for the electrical conductance of a single layer of SiSb (Figure 4(b)), exhibiting the utmost pinnacle of $\sigma = 1.623 \times 10^6 / \Omega m$ when measured at a temperature of 300 K.

Similar trends were observed for the thermal conductivities (κ) of the Si₂SbBi (Figure 3(c)) and SiSb (Figure 4(c)) monolayers, which were low. We obtained thermal conductivity values of 13.9918 W/mK and 13.3578 W/mK at $T = 300$ K for Si₂SbBi and SiSb, respectively. In both materials, thermal conductivity is affected by temperature, with higher temperature values corresponding to increased thermal conductivity levels. Strong electrical conductivity is paired with weak thermal conductivity, indicating favorable outcomes for the Seebeck coefficient and power factor of these materials.

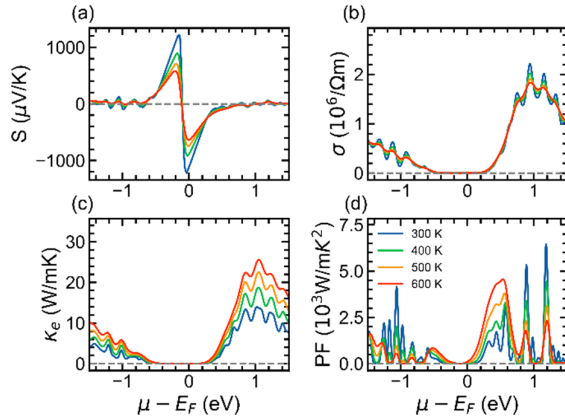


Figure 4. Seebeck coefficient (a), Electrical conductivity (b), Thermal conductivity (c), and Power Factor (d) of SiSb monolayer.

We also obtained the variation in the Seebeck coefficient (S) as a functional chemical at different temperatures of the Si₂SbBi monolayer, as shown in Figure 3(a). The figure shows that the Seebeck coefficient is affected by chemical potential and temperature. This aligns with Mott's formula [27]. Two peaks were observed around the Fermi level at each temperature. The highest peak value of the Seebeck coefficient was 1349 (1342) $\mu\text{V/K}$ for p -type (n -type) doping at 300 K, and it decreased with increasing temperature. The comprehensive Seebeck coefficient values obtained are 952.4 (1008) $\mu\text{V/K}$, 746.6 (829) $\mu\text{V/K}$, and 611.4 (710) $\mu\text{V/K}$ for p -type (n -type) doping at temperatures 400 K, 500 K, and 600 K, respectively.

We expanded our analysis beyond the Janus Si₂SbBi monolayer to include the Seebeck coefficient calculations for the SiSb monolayer. Figure 4(a) illustrates the temperature-dependent behavior of the SiSb monolayer, revealing intriguing insights. For the SiSb monolayer, we observed the highest peak of the absolute Seebeck coefficient to be 1198 (1198) $\mu\text{V/K}$ for the p -type (n -type) configuration, specifically at a temperature of 300 K. This data serves as a crucial benchmark for understanding the thermoelectric properties of the SiSb monolayer.

The Seebeck coefficient measures the electric voltage generated by a material in response to a temperature difference. As the temperature of the material increased, the particles became more energetic and produced a weaker voltage. Consequently, a temperature difference at higher temperatures causes a smaller voltage change, resulting in a lower Seebeck coefficient.

Using the thermal conductivity, electrical conductivity, and Seebeck coefficient values we obtained, we calculated the power factor (PF) using (6).

$$PF = S^2 \sigma \quad (6)$$

PF was plotted as a function of the chemical potential at different temperatures (T), as shown in Figure 3(d) for the Si₂SbBi monolayer. An interesting finding is that the PF increases as the temperature increases. This result is in contrast to that of the Seebeck coefficient, which

decreases as the temperature increases. The peak value of PF was $7 \times 10^3 \text{ W/mK}^2$ at 600 K for n -type doping.

A similar trend is also shown by the power factor of the SiSb monolayer (Figure 4(d)), which always increases with increasing temperature. PF value at 600 K shows a value close to $5 \times 10^3 \text{ W/mK}^2$ for p -type doping. Strengthening the Seebeck coefficient, the PF value of the Janus Si₂SbBi monolayer was greater than that of the SiSb monolayer. The polarization in a crystal system indirectly affects the thermoelectric properties of a material. These results indicate that the two-dimensional Janus Si₂SbBi material could be suitable as a TE material. With appropriate doping or functionalization, a material will increase the value of PF to describe the ZT value as a parameter-efficient electricity.

Our calculations have revealed an interesting finding regarding the Seebeck coefficient values of SiSb monolayer compared to Janus Si₂SbBi monolayer, as outlined in Table 2. It becomes apparent that the Seebeck coefficient value of the Janus Si₂SbBi monolayer surpasses not only the values we obtained for the SiSb monolayer in this study but also those for the SiBi monolayer from a prior work [10]. This observation underscores the superior thermoelectric potential held by the Janus Si₂SbBi monolayer within this comparative context.

Expanding this comparative landscape, our calculated Seebeck coefficient values for both the Janus Si₂SbBi and SiSb monolayers exhibit substantially higher magnitudes when juxtaposed with those of previously reported materials. Materials such as Be₃C₂, Be₃Si₂, Be₃Sn₂, Be₃Ge₂ [28], and the 2D ScX ($X = \text{P, As}$) materials (Table 2), demonstrate significantly lower Seebeck coefficient values compared to the ones derived from our calculations for the Si₂SbBi and SiSb monolayers. This discrepancy in Seebeck coefficient values highlights the potential superiority of the Janus Si₂SbBi monolayer for use in TE devices, with the PF parameter playing a pivotal role in substantiating this claim.

Moreover, delving deeper into this realm of exploration, the potential for experimental studies on the Janus Si₂SbBi monolayer material becomes increasingly apparent. This potential gets its inspiration from the successful characterization of Janus materials observed in Transition Metal Dichalcogenides (TMDC). This indicates a viable pathway for experimental investigations into the properties and applications of the Si₂SbBi monolayer Janus materials. This feasibility opens doors to empirical validations, paving the way for a more comprehensive understanding and practical utilization of these materials within the realm of thermoelectricity.

IV. CONCLUSION

In our study, we utilized DFT along with the Boltzmann theory to investigate the structural, electronic, and TE properties of two-dimensional Janus Si₂SbBi and non-Janus SiSb materials. The study showed that both Si₂SbBi and SiSb exhibit semiconductor behavior

characterized by bandgaps of 0.82 eV and 0.73 eV, respectively. By calculating the TE properties of the Janus Si₂SbBi, the Seebeck coefficient is found to be significantly enhanced, measuring 1349 $\mu\text{V/K}$ for *p*-type and 1342 $\mu\text{V/K}$ for *n*-type at 300 K. In addition, the electrical conductivity (σ) was determined to be $\sigma = 1.75 \times 10^6/\Omega\text{m}$ at ambient temperature. These parameters collectively contribute to a notable peak power factor (PF) of $4 \times 10^3 \text{W/mK}^2$. In comparison, the non-Janus SiSb monolayer exhibited lower values, including Seebeck coefficients of 1198 $\mu\text{V/K}$, electrical conductivity of $1.623 \times 10^6/\Omega\text{m}$, and a PF of $3 \times 10^3 \text{W/mK}^2$. In contrast, the Janus Si₂SbBi monolayer showed a significant improvement in both the Seebeck coefficient and PF, while exhibiting a reduced thermal conductivity, making it a highly competitive option for TE applications. This study presents a pioneering investigation of the TE properties of a two-dimensional Janus Si₂SbBi monolayer.

DECLARATIONS

Conflict of Interest

The authors have declared that no competing interests exist.

CRedit Authorship Contribution

Yusuf Affandi: Writing-Original Draft, Formal analysis; Funding acquisition; Muhammad Yusrul Hanna: Conceptualization, Methodology, Software, Data Curation.

Funding

Research reported in this publication was supported by PDP BIMA 2023, Ministry of Education, Culture, Research, and Technology, Republic of Indonesia, under grant number 113/E5/PG.02.00.PL/2023.

Acknowledgment

We acknowledge Mahameru BRIN for the use of its high-performance computing facilities in this work.

REFERENCES

- [1] M. A. Karri, E. F. Thacher, and B. T. Helenbrook, "Exhaust energy conversion by thermoelectric generator: two case studies," *Energy Convers. Manag.*, vol. 52, no. 3, pp. 1596–1611, Mar. 2011, doi: 10.1016/j.enconman.2010.10.013.
- [2] M. Aneke and M. Wang, "Energy storage technologies and real life applications – a state of the art review," *Appl. Energy*, vol. 179, pp. 350–377, Oct. 2016, doi: 10.1016/j.apenergy.2016.06.097.
- [3] J. Yang *et al.*, "On the tuning of electrical and thermal transport in thermoelectrics: an integrated theory-experiment perspective," *npj Comput. Mater.*, vol. 2, Feb. 2016, Art. no. 15015, doi: 10.1038/npjcompumats.2015.15.
- [4] Y. Tian and C. Y. Zhao, "A review of solar collectors and thermal energy storage in solar thermal applications," *Appl. Energy*, vol. 104, pp. 538–553, Apr. 2013, doi: 10.1016/j.apenergy.2012.11.051.
- [5] D. G. Cahill *et al.*, "Nanoscale thermal transport. II. 2003–2012," *Appl. Phys. Rev.*, vol. 1, no. 1, Mar. 2014, Art. no. 011305, doi: 10.1063/1.4832615.
- [6] B. Liao and G. Chen, "Nanocomposites for thermoelectrics and thermal engineering," *Mat. Res. Soc. Bull.*, vol. 40, no. 9, pp. 746–752, Sep. 2015, doi: 10.1557/mrs.2015.197.
- [7] Y. Affandi, M. A. U. Absor, and K. Abraha, "Effect of external electric field on spin-orbit splitting of the two-dimensional tungsten dichalcogenides WX₂ (X = S, Se)," in *J. Phys. Conf. Ser.*, vol. 1011, May 2018, Art. no. 012070, doi: 10.1088/1742-6596/1011/1/012070.
- [8] Y. Affandi and M. A. U. Absor, "Electric field-induced anisotropic Rashba splitting in two dimensional tungsten dichalcogenides WX₂ (X: S, Se, Te): a first-principles study," *Phys. E Low-Dimensional Syst. Nanostruct.*, vol. 114, Oct. 2019, Art. no. 113611, doi: 10.1016/j.physe.2019.113611.
- [9] M. Y. Hanna, E. H. Hasdeo, E. Suprayoga, and A. R. T. Nugraha, "Thermoelectric properties of two-dimensional hydrogenated borophene: a first-principles study," in *AIP Conf. Proc.*, vol. 2256, Sep. 2020, Art. no. 030017, doi: 10.1063/5.0014610.
- [10] K. Kaur, S. A. Khandy, S. Dhiman, U. B. Sharopov, and J. Singh, "Computational prediction of thermoelectric properties of 2D materials," *Electron. Struct.*, vol. 4, no. 2, Jun. 2022, Art. no. 023001, doi: 10.1088/2516-1075/ac635b.
- [11] J. O. Morales-Ferreiro, D. E. Diaz-Droguett, D. Celentano, and T. Luo, "First-principles calculations of thermoelectric properties of IV–VI chalcogenides 2D materials" *Front. Mech. Eng.*, vol. 3, Dec. 2017, Art. no. 15, doi: 10.3389/fmech.2017.00015.
- [12] J. H. Yang, Q. Yuan, H. Deng, S. H. Wei, and B. I. Yakobson, "Earth-abundant and non-toxic SiX (X = S, Se) monolayers as highly efficient thermoelectric materials," *J. Phys. Chem. C*, vol. 121, no. 1, pp. 123–128, Dec. 2017, doi: 10.1021/acs.jpcc.6b10163.
- [13] R. N. Somaiya, Y. A. Sonvane, and S. K. Gupta, "Exploration of the strain and thermoelectric properties of hexagonal SiX (X = N, P, As, Sb, and Bi) monolayers," *Phys. Chem. Chem. Phys.*, vol. 22, no. 7, pp. 3990–3998, Jan. 2020, doi: 10.1039/D0CP00002G.
- [14] S. Babaee Touski and N. Ghobadi, "Structural, electrical, and Rashba properties of monolayer Janus Si₂XY (X, Y = P, As, Sb, and Bi)," *Phys. Rev. B*, vol. 103, no. 16, Apr. 2021, Art. no. 165404, doi: 10.1103/PhysRevB.103.165404.
- [15] A. Lukmantoro and M. A. U. Absor, "Anisotropic Rashba splitting dominated by out-of-plane spin polarization in two-dimensional Janus XA₂Y (A = Si, Sn, Ge; X, Y = Sb, Bi) with surface imperfection," *Phys. Rev. Mater.*, vol. 7, no. 10, Oct. 2023, Art. no. 104005, doi: 10.1103/PhysRevMaterials.7.104005.
- [16] P. Giannozzi *et al.*, "QUANTUM espresso: a modular and open-source software project for quantum simulations of materials," *J. Phys. Condens. Matter*, vol. 21, no. 39, Sep. 2009, Art. no. 395502, doi: 10.1088/0953-8984/21/39/395502.
- [17] G. K. H. Madsen and D. J. Singh, "BoltzTraP. a code for calculating band-structure dependent quantities," *Comput. Phys. Commun.*, vol. 175, no. 1, pp. 67–71, Jul. 2006, doi: 10.1016/j.cpc.2006.03.007.
- [18] J. P. Perdew, K. Burke, and M. Ernzerhof, "Generalized gradient approximation made simple," *Phys. Rev. Lett.*, vol. 77, no. 18, pp. 3865–3868, Oct. 1996, doi: 10.1103/PhysRevLett.77.3865.
- [19] D. Vanderbilt, "Soft self-consistent pseudopotentials in a generalized eigenvalue formalism," *Phys. Rev. B*, vol. 41, no. 11, pp. 7892–7895, Apr. 1990, doi: 10.1103/PhysRevB.41.7892.
- [20] M. Kawamura, Y. Gohda, and S. Tsuneyuki, "Improved tetrahedron method for the Brillouin-zone integration applicable to response functions," *Phys. Rev. B - Condens. Matter Mater. Phys.*, vol. 89, no. 9, Mar. 2014, Art. no. 094515, doi: 10.1103/PhysRevB.89.094515.
- [21] H. J. Goldsmid and others, *Introduction to Thermoelectricity*. Springer Ser. Mat. Sci., vol. 121. Berlin, Heidelberg: Springer Berlin Heidelberg, 2010.
- [22] M. Khazaei, M. Arai, T. Sasaki, M. Estili, and Y. Sakka, "Two-dimensional molybdenum carbides: potential thermoelectric materials of the MXene family," *Phys. Chem. Chem. Phys.*, vol. 16, no. 17, pp. 7841–7849, Feb. 2014, doi: 10.1039/C4CP00467A.
- [23] A. Bafekry, F. Shojai, D. M. Hoat, M. Shahrokhi, M. Ghergherehchi, and C. Nguyen, "The mechanical, electronic, optical and thermoelectric properties of two-dimensional honeycomb-like of XSb (X = Si, Ge, Sn) monolayers: a first-principles calculations," *RSC Adv.*, vol. 10, no. 51, pp. 30398–30405, Aug. 2020, doi: 10.1039/d0ra05587e.
- [24] K. Kaur, D. Murali, and B. R. K. Nanda, "Stretchable and dynamically stable promising two-dimensional thermoelectric materials: ScP and ScAs," *J. Mater. Chem. A*, vol. 7, no. 20, pp. 12604–12615, Apr. 2019, doi: 10.1039/C9TA01393H.
- [25] A. F. Wani, B. Rani, S. Dhiman, U. B. Sharopov, and K. Kaur, "SiH monolayer: a promising two-dimensional thermoelectric material," *Int. J. Energy Res.*, vol. 46, no. 8, pp. 10885–10893,

- Mar. 2022, doi: 10.1002/er.7889.
- [26] M. G. Holland, "Analysis of lattice thermal conductivity," *Phys. Rev.*, vol. 132, no. 6, pp. 2461–2471, Dec. 1963, doi: 10.1103/PhysRev.132.2461.
- [27] M. Jonson and G. D. Mahan, "Mott's formula for the thermopower and the Wiedemann-Franz law," *Phys. Rev. B*, vol. 21, no. 10, pp. 4223–4229, May 1980, doi: 10.1103/PhysRevB.21.4223.
- [28] S. Nath, "Thermoelectric and optical properties of 2D hexagonal dirac material Be₃X₂ (X = C, Si, Ge, Sn): a density functional theory study," *J. Appl. Phys.*, vol. 130, Aug. 2021, Art. no. 55106, doi: 10.1063/5.0059942.